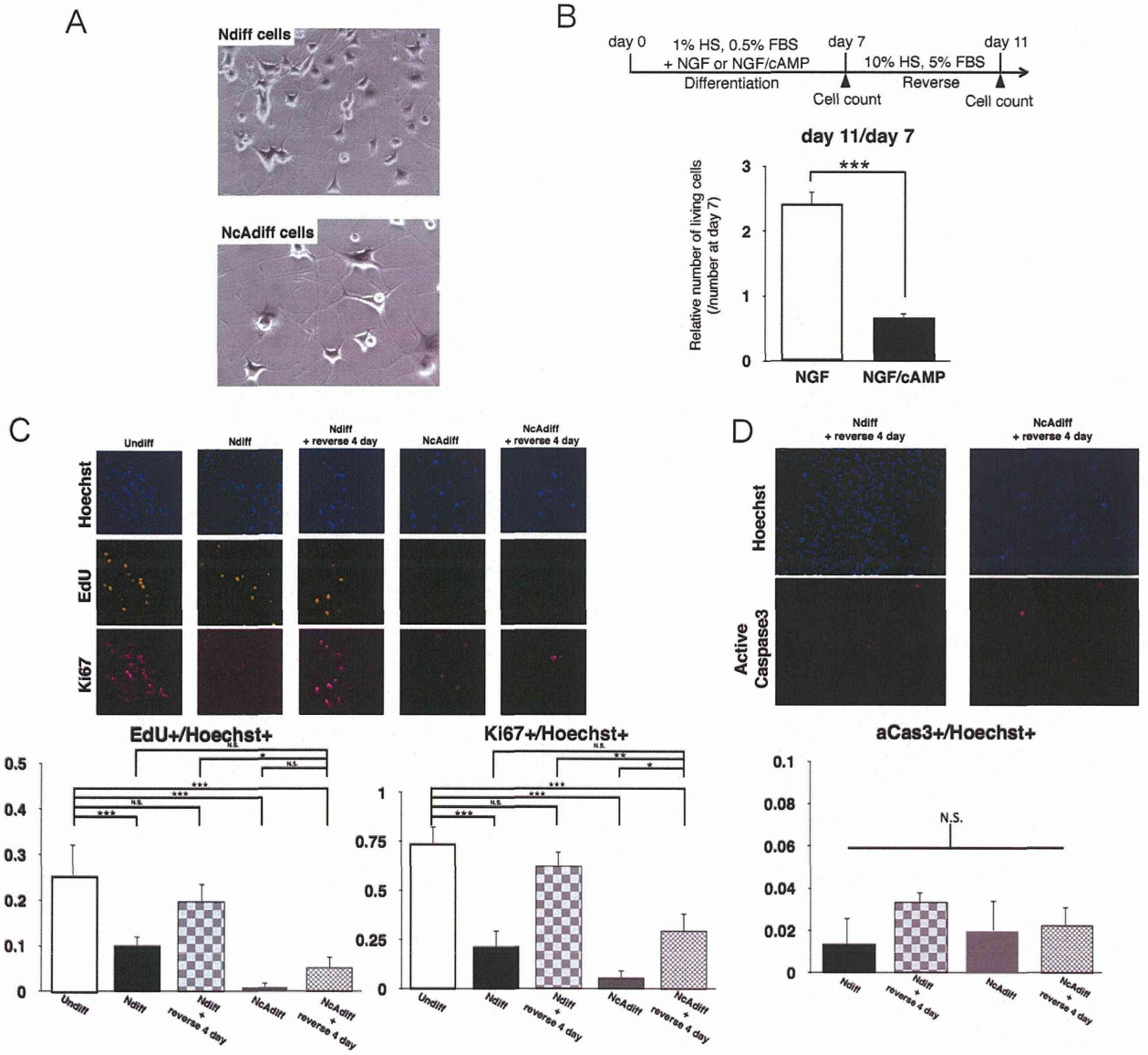


**Figure 1.** Combination of NGF and cAMP stimulations caused cell cycle arrest in differentiated PC12 cells. (**A**) Morphologies of PC12 cells that grew during 7 days of differentiation in the presence of NGF (upper) or NGF/cAMP (lower). (**B**) Relative number of living cells after removal of NGF or of NGF and cAMP. Upper diagram shows experimental scheme. After 7 days of differentiation of PC12 cells, NGF and cAMP were removed to allow proliferation. Number of living cells was evaluated by counting trypan blue staining-negative cells. Number of cells in each differentiation state at day 7 was set as 1. (**C**) Cell proliferation monitored by EdU incorporation and Ki67 staining in undifferentiated (Undiff), NGF-differentiated (Ndiff) and NGF/cAMP-differentiated (NcAdiff) cells, and in Ndiff and NcAdiff cells after 4 days of incubation in proliferative condition (Ndiff + reverse 4 day, NcAdiff + reverse 4 day, respectively). (**D**) Proportion of apoptotic cells before/after removal of NGF or NGF and cAMP, detected by active Caspase 3 (aCas3) staining. In (**B–D**), values are mean ± SD ($n = 3$). Statistical analysis was performed using Student's two-tailed $t$-tests, or the Tukey-Kramer multiple comparison test. N.S. = not significant. $^{*}P < 0.05$; $^{**}P < 0.01$; $^{***}P < 0.001$.

whether Ndiff and NcAdiff cells showed a difference in the reversibility of their differentiation after removal of these agents, we counted the number of cells after 7 days of differentiation in the presence of NGF or NGF/cAMP followed by 4 days of culture in proliferative conditions without NGF or cAMP (Figure 1B). After the NGF-containing differentiation medium was changed back to the proliferation medium, Ndiff cells resumed proliferation. In contrast, NcAdiff cells did not resume proliferation after such a change. Thus, 7 days of differentiation in the presence of NGF/cAMP induced irreversible differentiation of a fraction of PC12 cells, whereas the differentiation induced NGF alone was reversible. To monitor the cell cycle progression in each cell state, we immunostained incorporated 5-ethynyl-2′-deoxyuridine (EdU) and the proliferation marker Ki67 (Figure 1C). In Ndiff cells, both the EdU+

and the Ki67+ cells decreased by about 40%, compared to undifferentiated (Undiff) PC12 cells. After the NGF-containing differentiation medium was changed back to the proliferation medium, the fractions of both the EdU+ and the Ki67+ cells increased to levels comparable to those of Undiff cells. In contrast, the fractions of both the EdU+ and the Ki67+ cells were very low in NcAdiff cells. Even after the NGF/cAMP-containing differentiation medium was changed back to the proliferation medium, the fractions of both the EdU+ and the Ki67+ cells remained low. Thus, cells continued to proliferate marginally in the NGF-containing differentiation medium, whereas NcAdiff cells almost completely stopped progressing through the cell cycle. To investigate whether apoptosis occurred in each cell state, we immunostained an apoptosis marker, activated Caspase 3 (aCas3; Figure 1D). The fractions of aCas3+ cells were continuously very low, and did not differ markedly among all the samples examined. Taken together, these results showed that cell cycle arrest, but not apoptosis, occurred in the differentiated PC12 cells after the removal of cAMP.

### A significant number of M-phase-associated genes were specifically repressed in NcAdiff cells

To identify RNAs whose expression dynamics differed between reversibly and irreversibly differentiated PC12 cells, we performed high-throughput directional sequencing of Undiff, Ndiff and NcAdiff cells using Illumina Hiseq2000. The data contained over 148 million raw reads per sample, with a total of 517 million reads after removing low quality reads (Supplementary Table S4). These reads were mapped to the rat Rn5 reference genome using TopHat2 (see 'Materials and Methods' section). The average percentage of uniquely mapped reads among the valid reads was 81.7% (Supplementary Table S4). Our RNA-seq data showed little 5′-3′ mapping bias for annotated protein-coding genes (Ensembl gene annotation, version 76: Figure 2A) and robust reproducibility among four replicates (Pearson correlation coefficient, $R > 0.98$: Figure 2B). Hierarchical clustering analysis of the sequenced datasets based on the expression levels of protein-coding genes revealed that the expression profiles of protein-coding genes were cell-state-specific and highly reproducible among replicates (Figure 2C). In order to validate the strandedness of our directional RNA-seq data, we mapped the reads to the annotated RefSeq genes and calculated the proportion that mapped on the correct strand, and thereby found that more than 99% of the reads were mapped to the correct strands (Supplementary Table S5). In Ndiff cells, 3346 protein-coding genes showed significantly higher expression levels compared to those in NcAdiff cells ($q$-value $< 0.05$). Gene Ontology analysis of these Ndiff PC12-specific protein-coding genes revealed a strong enrichment in the Gene Ontology biological process terms associated with cell cycle, especially terms related to G2/M-phase progression (e.g., mitotic cell cycle, M phase and mitotic M phase: Figure 2D), which is consistent with our finding that cell cycle arrest was observed much more frequently in NcAdiff cells than in Ndiff cells (Figure 1C).

### pancRNA and mRNA pairs were possible downstream targets of cAMP signaling pathway

Impey *et al.* reported that more than half of total pCreb1-binding sites are located adjacent to genes, and in particular, pCreb1-binding regions are significantly enriched in bidirectional promoters that produce annotated transcripts in both directions (annotated bidirectional promoters or aBiPs) (15). Recent studies have revealed that antisense noncoding transcripts are derived from upstream of many protein-coding genes in mammals (7,11,37). We therefore hypothesized that not only aBiPs, but also protein-coding gene promoters that simultaneously produce pancRNAs (pancRNA-associated bidirectional promoters or pBiPs) were potential targets of transcriptional regulation by a CRE-mediated mechanism.

To test our hypothesis, first, we adjusted the annotated TSSs of genes according to our directional RNA-seq data in order to improve the accuracy of prediction of pBiPs (see 'Materials and Methods' section). Next, because MACS2 showed more sensitivity and accuracy for detection of lncRNA than transcript models reconstructed using *ab initio* transcript assembly tools (e.g. Cufflinks and Trinity; Supplementary Figure S2), we identified the read-enriched regions using MACS2 software after parameter setting, and classified these regions according to their positions relative to those of annotated transcripts. A total of 51 939 regions were classified as regions of non-annotated transcripts. Of these, 2758 regions were classified as regions of candidate-pancRNAs, which were overlapped with the 1-kb region upstream of the TSS of an annotated protein-coding gene in an antisense direction. The average length of the candidate-pancRNAs was 1928 bp, and the average distance between the 5′ ends of candidate-pancRNAs and that of its partnered gene was 167 bp (Supplementary Figure S3). As expected, based on coding potential estimation using the CPC algorithm (27), 92.5% of the non-annotated transcripts and 96.9% of candidate-pancRNAs exhibited negative coding potential scores, suggesting that most of these regions can be regarded as templates of pancRNAs (Figure 3A). We regarded the annotated protein-coding gene promoters producing pancRNAs as pBiPs. As a result, we identified 3235 bidirectional promoters in PC12 cells. Of these, 948 genes derived from 474 out of 477 aBiPs, 2718 pancRNAs and their paired genes derived from 2718 out of 2758 pBiPs were transcribed in Undiff, Ndiff or NcAdiff cells.

Then, we investigated the frequency of CRE occurrence in aBiPs and pBiPs. There were one or more CRE sequences in 27.6% of all protein-coding gene promoters (−1000 to +1000 bp from the TSS) and in 36.1% of aBiPs and 32.3% of pBiPs. Thus, in agreement with our hypothesis, CRE sequences were highly enriched not only in aBiPs, but also in pBiPs compared to all protein-coding gene promoters (Figure 3B). To further validate our hypothesis, we analyzed a publicly available pCreb1 ChIP-seq dataset of PC12 cells immediately after cAMP signal activation by forskolin (15). Investigation of the frequency of overlap of pCreb1-binding at protein-coding gene promoters showed that pCreb interacted with 59% of aBiPs, 45% of pBiPs and 23% of all protein-coding gene promoters. Similarly, we analyzed a publicly available Creb1 ChIP-seq dataset of E16.5 mouse

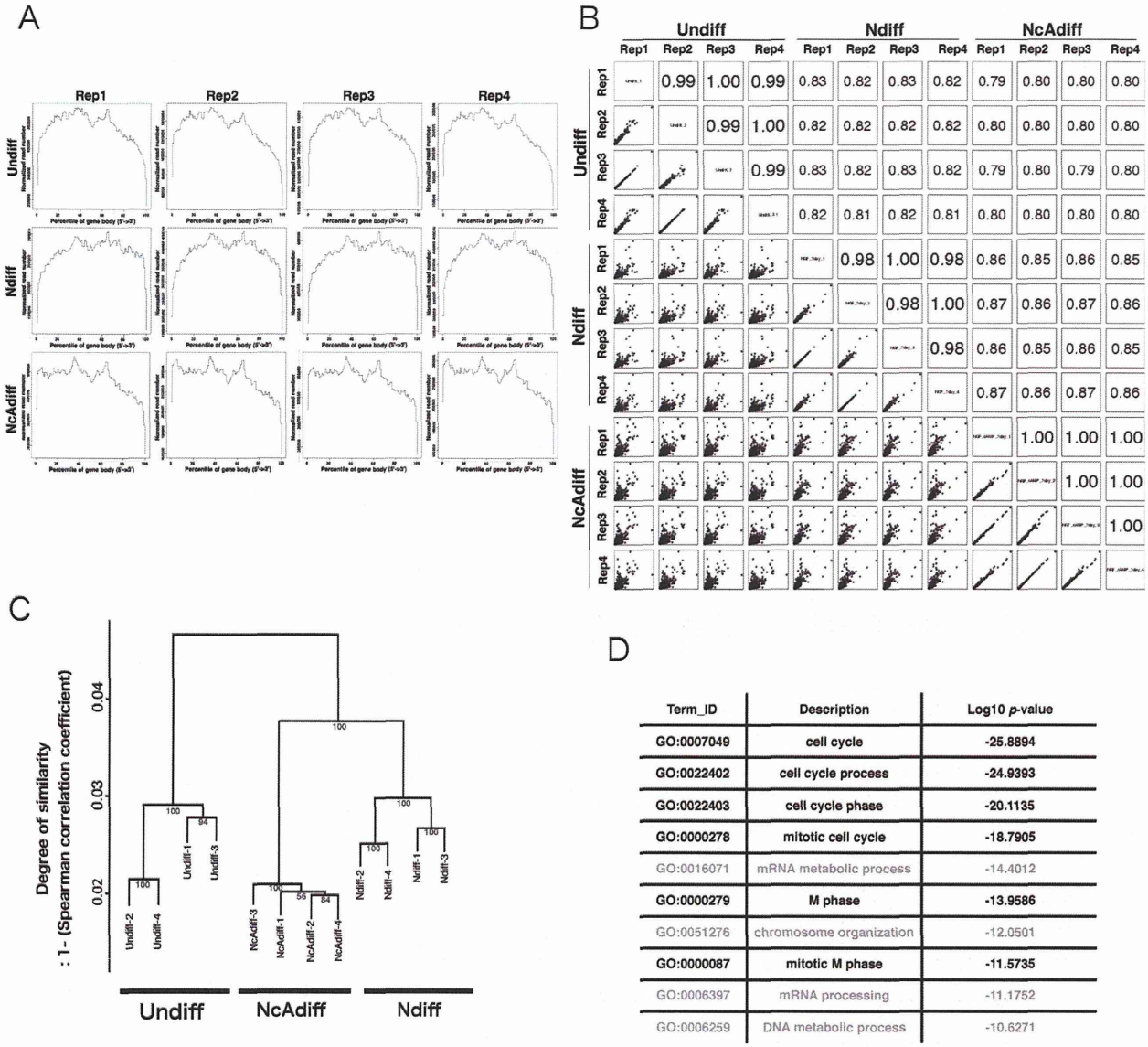


| Term_ID | Description | Log10 *p*-value |
|---|---|---|
| **GO:0007049** | **cell cycle** | **-25.8894** |
| **GO:0022402** | **cell cycle process** | **-24.9393** |
| **GO:0022403** | **cell cycle phase** | **-20.1135** |
| **GO:0000278** | **mitotic cell cycle** | **-18.7905** |
| GO:0016071 | mRNA metabolic process | -14.4012 |
| **GO:0000279** | **M phase** | **-13.9586** |
| GO:0051276 | chromosome organization | -12.0501 |
| **GO:0000087** | **mitotic M phase** | **-11.5735** |
| GO:0006397 | mRNA processing | -11.1752 |
| GO:0006259 | DNA metabolic process | -10.6271 |

**Figure 2.** A significant number of M-phase associated genes were not stringently repressed in Ndiff cells. (**A**) Density plots of directional RNA-seq reads mapped to the RefSeq genes to evaluate 5′-3′ potential mapping bias across genes. Each sample category consisted of four replicates (Rep1–4). (**B**) Scatter plots of gene expression levels and Pearson correlation coefficients among all sequenced samples. The expression levels of genes were calculated based on the number of reads mapped to each Ensembl protein-coding gene normalized by iDEGES/edgeR methods. (**C**) Hierarchical clustering of sequence data sets based on the expression levels of Ensembl protein-coding genes. The distance between samples was determined by clustering using group average methods and linkage criteria based on Spearman's rank coefficient of correlation. The numbers in tree diagrams are approximately unbiased *P*-values. (**D**) The top 10 most significantly enriched GO terms for 3346 Ndiff-specific protein-coding genes. The *P*-value is the Benjamini–Hochberg corrected *P*-value.

cortical neurons that had been maintained *in vitro* for 7 days (32). Creb1 binding signals were significantly enriched not only in aBiPs, but also in pBiPs (Supplementary Figure S4). These results supported our hypothesis that not only aBiPs but also pBiPs were preferred downstream targets of cAMP signaling during the irreversible differentiation of PC12 cells.

Next, because the expression of pancRNA and the corresponding annotated protein-coding gene are positively correlated in both mouse and human brain (11,38), we investigated whether the expression dynamics of pancRNA–mRNA pairs were also positively correlated during the differentiation of PC12 cells. First, we calculated the correlation coefficient of the expression level of each RNA pair during PC12 differentiation, and then classified them into three groups. The first group was composed of antisense lncRNAs that overlapped with the 1-kb region upstream from the 5′ ends of mRNAs and the partner mRNAs (pancRNA–mRNA pairs). The second group was composed of antisense lncRNAs that overlapped with the 1-

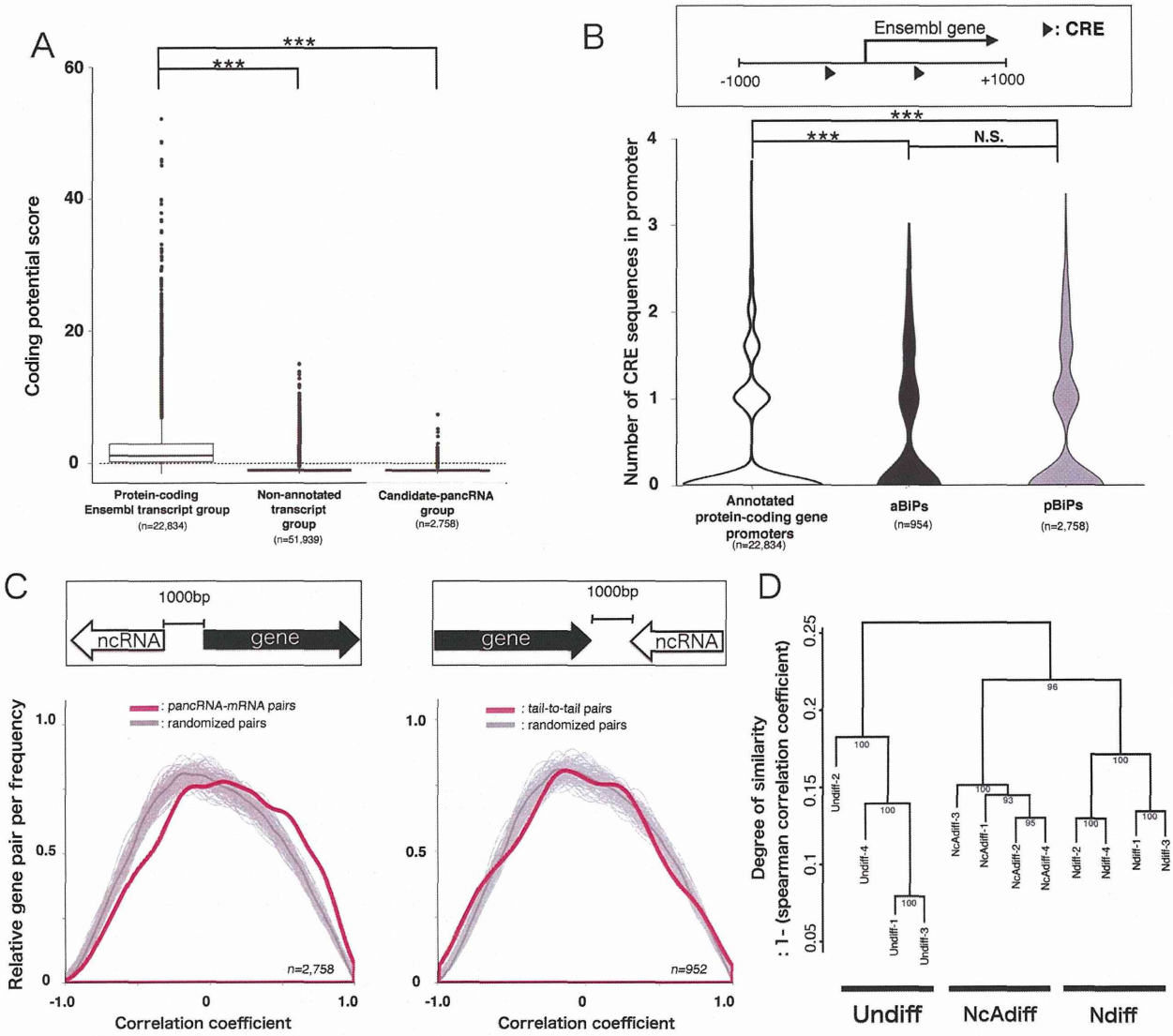


**Figure 3.** The bidirectional promoters driving pancRNAs can be novel targets of cAMP signaling. (**A**) Distribution of coding potential scores for annotated protein-coding Ensembl transcripts, non-annotated transcripts and candidate-pancRNAs using the CPC algorithm. Negative scores indicate low coding potential. (**B**) Distribution of numbers of CREs located in the promoters (−1000 to +1000 from TSS) of all protein-coding genes, genes derived from aBiPs and pBiPs. (**C**) Distribution of Pearson correlation coefficients calculated based on the expression of protein-coding genes and nearest novel lncRNAs (magenta curve). The dark gray lines show the average correlation coefficient distribution based on 200 permutations of 2000 randomly selected pairs of lncRNAs and protein-coding gene. The pale gray lines represent 200 simulation results. Significance was calculated with the Mann–Whitney U test (left: $P < 2.2e\text{-}16$; right: $P = 0.59$). (**D**) Hierarchical clustering of sequence data sets based on pancRNA expression levels. The distance between samples was determined by clustering using group average methods and linkage criteria based on Spearman's rank coefficient of correlation. The numbers in tree diagrams are approximately unbiased *P*-values. Statistical analysis was performed using the Tukey-Kramer multiple comparison test in (A and B). N.S. = not significant. $***P < 0.001$.

kb region downstream from the 3′ ends of mRNAs and the partner mRNAs (tail-to-tail pairs). The third group was composed of randomly selected RNA transcripts (randomized pairs). We found that the distribution of the correlation coefficients of the pancRNA–mRNA pairs was significantly different from that of the tail-to-tail pairs (Bonferroni-corrected Mann–Whitney U test, $P < 2.1e\text{-}9$) and that of randomized pairs ($P < 2e\text{-}16$; Figure 3C left). However, no significant difference was observed between the distribution of the correlation coefficients of the tail-to-tail pairs and that of randomized pairs ($P = 0.99$; Figure 3C right). These statistical analyses highlighted the positive correlation of pancRNA–mRNA expression during PC12 differentiation. The hierarchical clustering analysis of sequenced datasets based on candidate-pancRNA expression levels revealed that the expression profiles of candidate-pancRNAs were cell-state-specific and highly reproducible among replicates (Figure 3D). These genome-wide analyses supported

the notion that pancRNAs are physically associated with cAMP targets for the partner gene activation.

### After irreversible differentiation, both *Nusap1* and *pancNusap1* expression levels, and the histone acetylation level of the *Nusap1* promoter, were dramatically decreased

Among candidate-pancRNAs, we then focused on a pancRNA from the promoter of a spindle-formation-associated gene *Nusap1* in an attempt to elucidate possible functions of this pancRNA. This pancRNA and its paired annotated protein-coding gene pair exhibited the highest Pearson correlation coefficient among all pancRNA–mRNA pairs during PC12 differentiation ($P = 0.995$: Figure 4A). However, the RNA-seq data showed that there was no coordination of the expression changes of any *Nusap1*-neighboring genes with that of *Nusap1* and its pancRNA (Supplementary Figure S5). We named this pancRNA *pancNusap1*. Its expression as estimated by RNA-seq analysis was lowest in NcAdiff cells among all of the cell samples examined. TGACG, one of the previously identified non-canonical CREs (15), was symmetrically located at −12 and −380 bp relative to the TSS of *Nusap1* (Figure 4C, black arrowheads). Similarly, CGCCA (33) was located at +31 and −230 bp relative to the TSS of *Nusap1* (Figure 4C, gray arrowheads, Supplementary Figure S6). These non-canonical CREs also appeared near the *Nusap1* TSS in the mouse and human genomes (Supplementary Figure S6). We then examined the expression patterns of *pancNusap1* and *Nusap1* in each differentiation state of PC12 cells. As shown in Figure 4B, the expression dynamics of *pancNusap1* as determined by RT-qPCR seemed to be positively correlated with those of *Nusap1*. We confirmed that the expression levels of both *Nusap1* and *pancNusap1* were significantly lower in NcAdiff cells than in Ndiff cells. Interestingly, these lower levels of *pancNusap1* and *Nusap1* expression seemed to continue after NcAdiff cells were put back under proliferative conditions. That is, after the NGF-containing differentiation medium was changed back to the proliferation medium, the expression levels of both *Nusap1* and *pancNusap1* in Ndiff cells recovered to a level similar to that in Undiff cells, whereas the expression levels of both *Nusap1* and *pancNusap1* in NcAdiff cells failed to fully recover after 4 days in proliferative condition.

Since we reported that the expression changes of pancRNAs caused a regional alteration in the epigenetic states in the pBiPs (8), next we examined the epigenetic state of the *Nusap1* promoter by means of bisulfite sequencing and ChIP-qPCR assay. The DNA methylation states were not changed upon differentiation in PC12 cells (Figure 4C). However, the levels of active histone modifications, such as histone H3 lysine 9 acetylation (H3K9ac) and lysine 27 acetylation (H3K27ac), were lower in NcAdiff cells than in Undiff and Ndiff cells (Figure 4D and E). The levels of signals of H3K9ac and H3K27ac on the *Nusap1* promoter in NcAdiff cells remained very low after the differentiation medium was changed back to the proliferation medium (Figure 4E). These kinetics of the histone acetylation levels were concordant with the *pancNusap1* expression pattern, raising the possibility that *pancNusap1* is required for local open chromatin formation, and cessation of the expression of *pancNusap1* causes histone deacetylation at the *Nusap1* promoter. Histone methylation levels, such as the active histone modification histone H3 lysine 4 trimethylation (H3K4me3), and the repressive histone modifications histone H3 lysine 9 tri-methylation (H3K9me3) and lysine 27 tri-methylation (H3K27me3), were not different between Ndiff and NcAdiff cells (Figure 4D). Taken together, these results indicate that *pancNusap1* expression is associated with local histone acetylation specifically in a cAMP-minus condition.

### Knockdown of *pancNusap1* induced a closed chromatin structure in the *Nusap1* promoter, resulting in cell cycle arrest

To test the hypothesis that the regulation of *pancNusap1* is critical for irreversible differentiation, first we examined the effects of *pancNusap1* KD on the expression levels of *Nusap1* in the cells under reversible differentiation condition (see 'Materials and Methods' section). Both of the tested shRNAs for *pancNusap1* downregulated the expressions of not only *pancNusap1* but also *Nusap1* in Ndiff cells (Figure 5A and Supplementary Figure S7). We confirmed that neither of the shRNAs for *pancNusap1* showed off-target effects (Supplementary Figure S8). Next, we investigated the effect of *pancNusap1*-KD on the histone acetylation profile in the *Nusap1* promoter. ChIP-qPCR analysis revealed that *pancNusap1*-KD significantly decreased the signals of both H3K9ac and H3K27ac in the *Nusap1* promoter without affecting the signal levels in the *Gapdh* promoter (Figure 5B and Supplementary Figure S9). Then we examined whether *pancNusap1*-KD affected the proliferation of Ndiff cells after they were returned to the proliferation medium. Counting the living cells revealed that *pancNusap1*-KD inhibited the proliferation of Ndiff cells after the NGF-containing differentiation medium was changed to the proliferation medium (Figure 5C). Moreover, consistent with our hypothesis, immunostaining showed that *pancNusap1*-KD decreased both the EdU+ and the Ki67+ cells even after the NGF-containing differentiation medium was changed back to the proliferation medium (Figure 5D). Thus, repression of *pancNusap1* mimics the epigenetic features of irreversibly differentiated PC12 cells.

### Overexpression of *pancNusap1* induced cell cycle progression with an open chromatin formation in the *Nusap1* promoter

To further test our hypothesis that regulation of *pancNusap1* is critical for irreversible differentiation, we examined the effects of *pancNusap1* OE on the expression levels of *Nusap1* in NcAdiff cells. Since *pancNusap1* contained regions highly homologous with mouse *Oip5* (Figure 6A), it seemed possible that this pancRNA might need to be translated in order for it to function. However, when we used a genomic region lacking the predicted translation initiation site (*pancNusap1ΔTIS*), we still found upregulation of *Nusap1* (Figure 6B). Because we discovered previously that several pancRNAs function in a strand-specific manner (8), we also prepared PC12 cells in which the strand opposite *pancNusap1* (*sense_pancNusap1ΔTIS*) was exogenously expressed (Figure 6A), and found that

A

| Ensembl gene ID : gene name | Correlation coefficient | Normalized read counts of pancRNA in Ndiff cells | Normalized read counts of pancRNA in NcAdiff cells | $Log_2$(Ndiff/ NcAdiff) |
|---|---|---|---|---|
| ENSRNOG00000004921:Nusap1 | 0.996 | 1142.340 | 373.754 | 1.612 |
| ENSRNOG00000013920:Arhgap26 | 0.979 | 1300.450 | 2337.300 | -0.846 |
| ENSRNOG00000012347:Gata2 | 0.970 | 20971.300 | 8365.470 | 1.326 |
| ENSRNOG00000010435:Nupl2 | 0.970 | 277.657 | 176.517 | 0.653 |
| ENSRNOG00000021839:RGD1563556 | 0.967 | 615.537 | 253.741 | 1.278 |
| ENSRNOG00000016534:Fam171a1 | 0.962 | 3277.990 | 8169.870 | -1.318 |
| ENSRNOG00000027249:Fancl | 0.956 | 85.277 | 35.207 | 1.276 |
| ENSRNOG00000020274:Taf5 | 0.951 | 365.662 | 212.179 | 0.785 |
| ENSRNOG00000049849:Fam199x | 0.941 | 464.205 | 309.653 | 0.584 |
| ENSRNOG00000005332:Csdc2 | 0.940 | 1145.180 | 2045.300 | -0.837 |

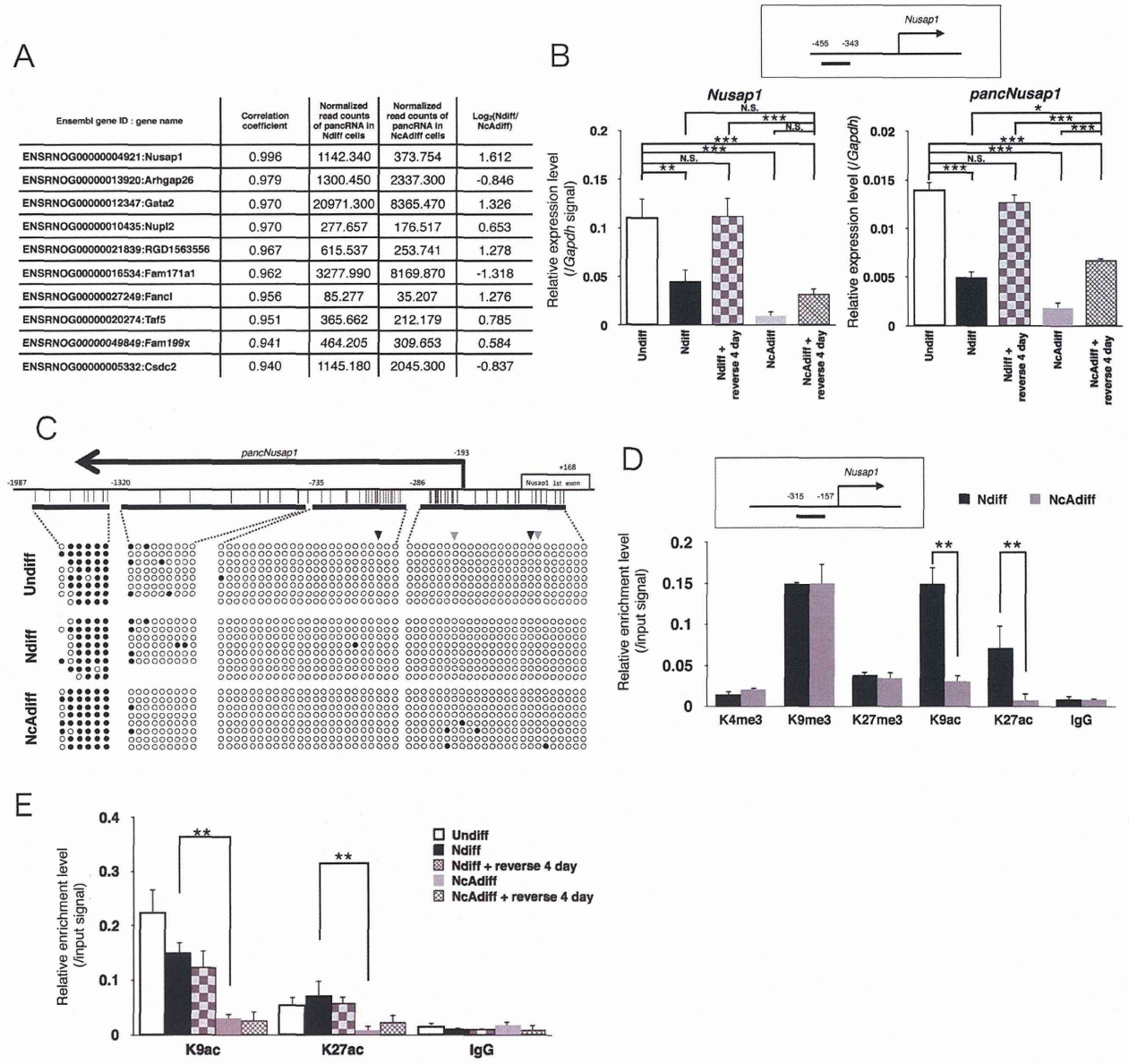


**Figure 4.** Both *Nusap1* and *pancNusap1* were epigenetically repressed in NcAdiff cells. (**A**) List of the top 10 candidate-pancRNA/mRNA pairs showing highest correlation of expression during PC12 differentiation. The expression levels of pancRNAs normalized with the iDEGES/edgeR method are also shown. (**B**) RT-qPCR analysis of *pancNusap1* and *Nusap1* in Undiff, Ndiff and NcAdiff cells, before and after NGF and cAMP factor deprivation. Upper diagram shows the location of the primer used for RT-qPCR of *pancNusap1*. *Gapdh* was used as a control. (**C**) DNA methylation levels of the *Nusap1* promoter region in Undiff, Ndiff and NcAdiff cells. Upper diagram shows the genomic structure of the rat *Nusap1* promoter. Thick horizontal lines indicate the regions analyzed by bisulfite sequencing. Vertical lines mark the location of CpG dinucleotides. Primer positions are numbered relative to TSS of the *Nusap1* gene. Filled and empty circles indicate methylated and unmethylated cytosines, respectively. Black and gray arrowheads indicate locations of the previously identified non-canonical CRE, TGACG and CGCCA, respectively. (**D** and **E**) Histone modification status of the *Nusap1* promoter in each differentiation state of PC12 cells. Upper diagram shows the location of the primers used in the ChIP assay. Status of histone H3 lysine 4 tri-methylation (H3K4me3), lysine 9 tri-methylation (H3K9me3), lysine 27 tri-methylation (H3K27me3), histone H3 lysine 9 acetylation (H3K9ac) and lysine 27 acetylation (H3K27ac) was evaluated. Normal mouse IgG (IgG) was used as a negative control. The same amount of chromatin fragments as used for each immunoprecipitation was also subjected to PCR without IP as a positive control (Input). In (B), (D) and (E), values are mean ± SD ($n = 3$). Statistical analysis was performed using Student's two-tailed *t*-tests, or the Tukey-Kramer multiple comparison test. N.S. = not significant. $^{**}P < 0.01$; $^{***}P < 0.001$.

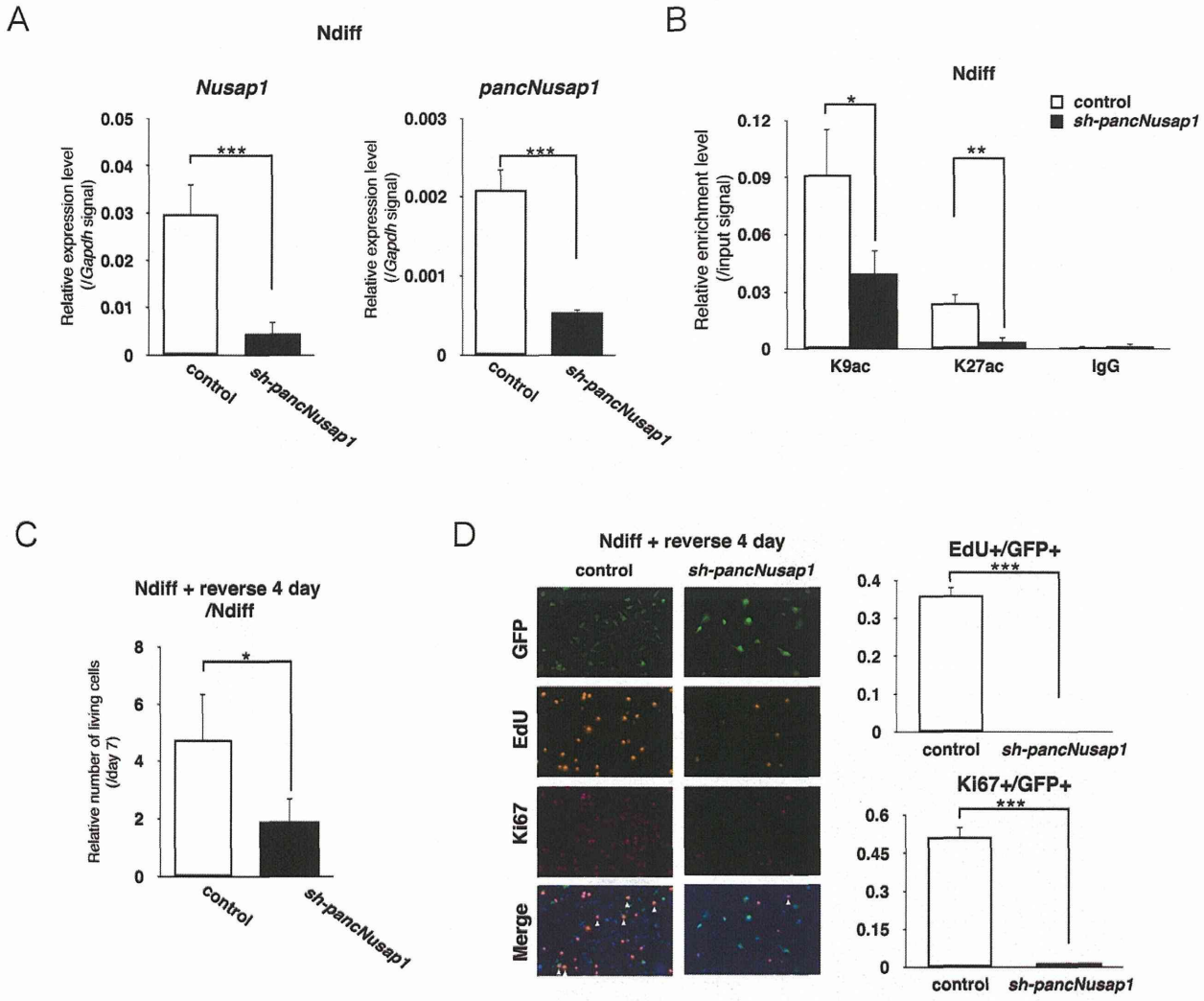


**Figure 5.** Knockdown (KD) of *pancNusap1* mimicked irreversible differentiation of PC12 cells induced by cAMP (**A**) The effect of *pancNusap1* KD on the expression level of *Nusap1* in Ndiff cells. *Gapdh* was used as a control. Empty vector-introduced PC12 cells were used as a negative control. (**B**) Histone modification status of the *Nusap1* promoter in *pancNusap1*-KD PC12 cells under reversible differentiation condition. The expression of *sh-pancNusap1* was induced by Dox at day 5. Empty vector-infected PC12 cells were used as a control. (**C**) The effects of *pancNusap1* KD on cell proliferation in Ndiff cells. The numbers of living cells were counted. (**D**) Proportion of the EdU+ and the Ki67+ cells in *pancNusap1*-KD PC12 cells after NGF deprivation. After 7 days of differentiation, NGF was removed to allow proliferation. White arrowheads indicate locations of proliferating infected cells (triple-positive for Ki67, EdU and GFP). In (A–C), viral vectors were introduced at day 3. In (A–D), values are mean ± SD ($n = 3$). Statistical analysis was performed using Student's two-tailed *t*-tests, or the Tukey-Kramer multiple comparison test. N.S. = not significant. $*P < 0.05$; $**P < 0.01$; $***P < 0.001$.

the introduction of *sense_pancNusap1ΔTIS* could not upregulate the expression of *Nusap1* (Figure 6B). This indicates that the direction of transcription of this pancRNA was important for its function as a local gene activator. We also investigated the effect of *pancNusap1ΔTIS*-OE and *sense_pancNusap1ΔTIS*-OE on the histone acetylation profile of the *Nusap1* promoter in NcAdiff cells, and found that *pancNusap1ΔTIS*-OE, but not *sense_pancNusap1ΔTIS*-OE, increased the signals of both H3K9ac and H3K27ac at the *Nusap1* promoter in parallel with *Nusap1* upregulation (Figure 6C). Then, to investigate the effects of *pancNusap1*-OE on the phenotypic irreversibility of PC12 cells, we immunostained PC12 cells with antibody against Ki67 and counted the number of living cells before/after the NGF/cAMP-containing medium was changed back to the proliferation medium, and found that the number of cells was increased by *pancNusap1ΔTIS*-OE, but not by *sense_pancNusap1ΔTIS*-OE (Figure 6A and D). Immunostaining revealed an increase of the Ki67+ cells after *pancNusap1ΔTIS*-OE (Figure 6E), indicating that re-proliferation was enhanced by *pancNusap1ΔTIS*-OE. These data showed that *pancNusap1ΔTIS*-OE expression could induce morphological and epigenetic features characteristic of the reversibly differentiated state of PC12 cells in irreversibly differentiated cells.

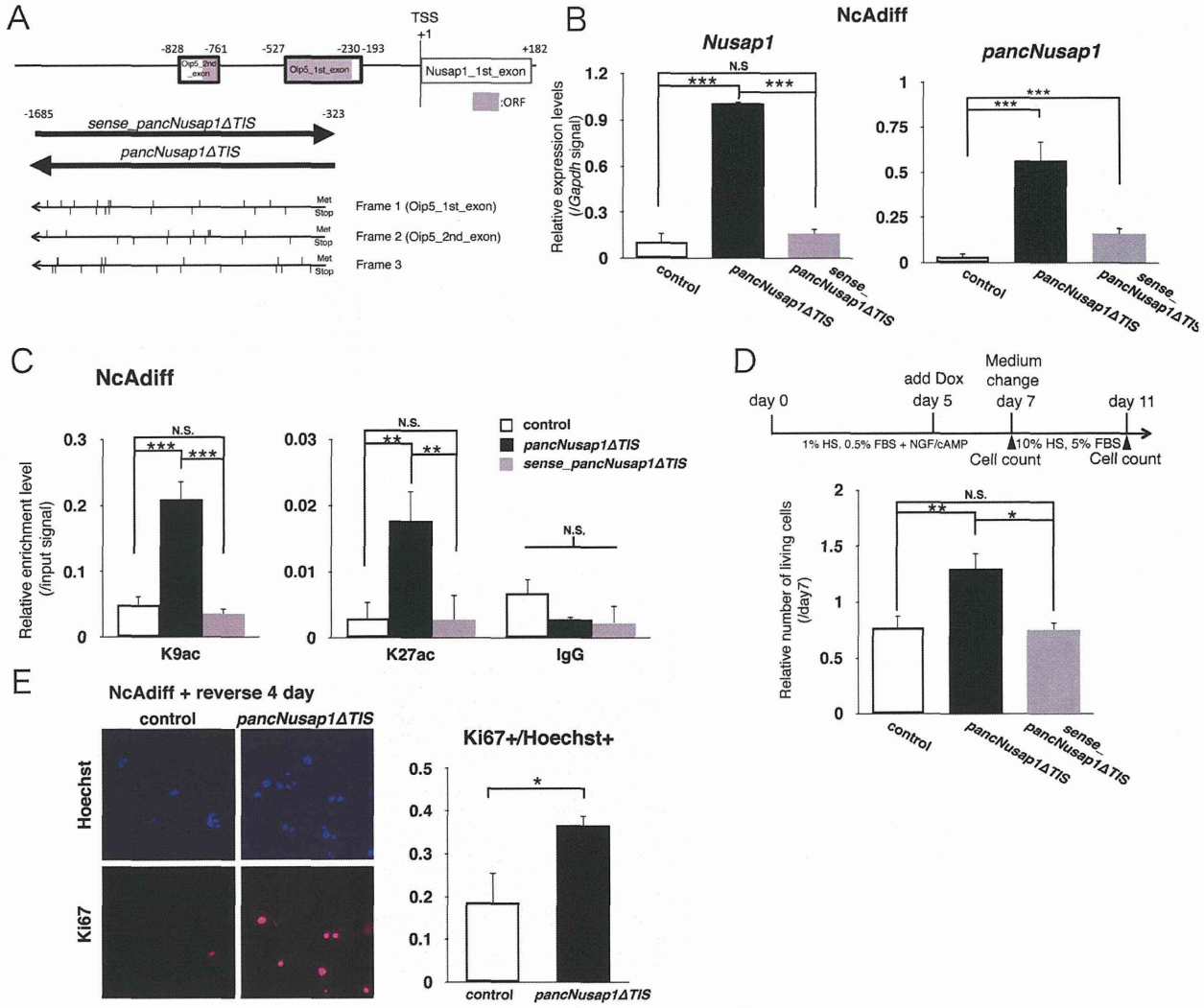


**Figure 6.** *pancNusap1* overexpression (OE) caused cells subjected to the irreversibly differentiation condition to have the morphological and epigenetic characters of reversibly differentiated cells. (**A**) Genomic structure of the rat *Nusap1* promoter. Bold-lined boxes show the region homologous to mouse *Oip5*. Gray boxes indicate predicted locations composing the *Oip5* open reading frame (ORF). Lower thick arrows indicate the region and transcribed strands used for OE-experiments of ncRNA. Upper and lower vertical lines show the positions of methionines (Met) or stop codons (Stop), respectively, in each translational frame. (**B**) The effect of Dox-induced sense or antisense *pancNusap1* OE on the *Nusap1* expression level in NcAdiff cells. *Gapdh* was used as a control. Empty vector-introduced PC12 cells were used as a negative control. (**C**) Histone modification status of the *Nusap1* promoter in *pancNusap1*-overexpressing PC12 cells under irreversible differentiation condition. (**D**) The effect of Dox-induced sense or antisense *pancNusap1* OE on cell proliferation in NcAdiff cells. Upper diagram shows experimental scheme. Number of living cells was counted. After 7 days of differentiation of PC12 cells, NGF/cAMP were removed to allow proliferation. (**E**) Proportion of Ki67+ cells in antisense *pancNusap1*-overexpressing PC12 cells after NGF/cAMP deprivation. In (B–E), values are mean ± SD ($n = 3$). Statistical analysis was performed using Student's two-tailed *t*-tests or the Tukey-Kramer multiple comparison test. N.S. = not significant. $*P < 0.05$; $**P < 0.01$; $***P < 0.001$.

### Overexpression of *Nusap1* rescued *pancNusap1*-KD-induced cell cycle arrest

To test the epigenetic effects of *pancNusap1*-KD and -OE in a single gene expression setting, we performed rescue experiments of *pancNusap1*-KD cells with *Nusap1*-OE, and monitored the proliferation of Undiff or Ndiff cells after introduction of *sh-pancNusap1* and *Nusap1*. In Undiff cells, the reductions of both the EdU+ and the Ki67+ cells by *pancNusap1*-KD were rescued by the simultaneous introduction of *Nusap1*-OE (Figure 7A and Supplementary Figure S10). Counting the number of living cells after 4 days of culture in re-proliferative condition further confirmed that, after the NGF-containing differentiation medium was changed back to the proliferation medium, the reduction of the number of cells by *pancNusap1*-KD was successfully rescued by simultaneous *Nusap1*-OE expression (Figure 7B). These results clearly indicate that *pancNusap1* acts to up-regulate the transcription of *Nusap1*.

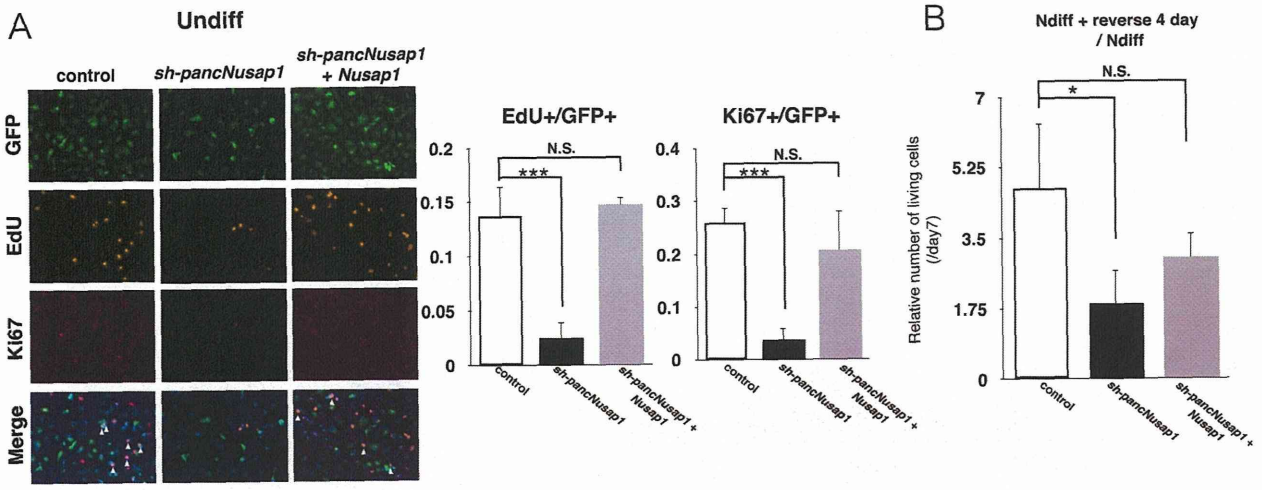


**Figure 7.** *pancNusap1* regulates irreversibility of PC12 differentiation through transcriptional regulation of *Nusap1*. (**A**) Proportion of the EdU+ and the Ki67+ cells in *pancNusap1*-KD and *Nusap1*-OE Undiff cells. White arrowheads indicate locations of the proliferating infected cells (triple-positive for Ki67, EdU and GFP). (**B**) The effect of *Nusap1*-OE on cell proliferation in the *pancNusap1*-KD cells. Number of living cells was counted. In (A and B), values are mean ± SD ($n = 3$). Statistical analysis was performed using the Tukey-Kramer multiple comparison test. N.S. = not significant. $*P < 0.05$; $***P < 0.001$.

### The activities of pBiPs, including that for the *pancNusap1-Nusap1* pair, were regulated by cAMP signaling

By using the publicly available pCreb1 ChIP-seq dataset of PC12 cells (15), we found that pCreb1 interacted with the *Nusap1* promoter immediately after cAMP signal activation by forskolin. However, because *pancNusap1* and *Nusap1* were silenced in response to cAMP stimulation in NcAdiff cells (Figure 4B), we tried to experimentally confirm the pCreb1-binding at the *Nusap1* promoter and to identify the factors that shut down cAMP-dependent activation of the *pancNusap1–Nusap1* pair as well. Some reports showed that transcription of a dominant-negative form of *Crem*, *Icer* (Supplementary Figure S11A), is activated by binding of pCreb1 after cAMP treatment in PC12 cells (19,39), and therefore we investigated the transcriptional dynamics of *Creb1*, *Crem* and *Icer* using our RNA-seq data. Consistent with previous reports, we found that transcription of *Icer* was dramatically activated in NcAdiff cells (Supplementary Figure S11B). We confirmed these results by RT-qPCR (Supplementary Figure S11C). Next, we performed time-course ChIP experiments to examine the binding of pCreb1 and Icer to the *Nusap1* promoter after NGF/cAMP treatment (Figure 8A). We found that pCreb1-binding was upregulated at 3 h and then diminished by 72 h after the NGF/cAMP treatment. In contrast, Icer-binding was upregulated at 3 h but then partially maintained until 72 h after the NGF/cAMP treatment. These ChIP-qPCR data agree well with the RT-qPCR data, in which both *Nusap1* and *pancNusap1* transcripts were reduced to the basal levels by 72 h (Figure 8B). To further validate the differential roles of pCreb1 and Icer in the transcriptional regulation of the *Nusap1* promoter during PC12 differentiation, we examined the effects of *Icer* and *Creb1* KD on the expression levels of *Nusap1* and *pancNusap1*. As expected, our shRNAs specifically targeted *Icer* or *Creb1*, resulting in their significant downregulation (Figure 8C and Supplementary Figure S12). KD of *Icer* upregulated the expression levels of both *pancNusap1* and *Nusap1* in NcAdiff cells (Figure 8D). In contrast, KD of *Creb1* did not affect the expression levels of either *Nusap1* or *pancNusap1* in NcAdiff cells (Figure 8D). Taking these results all together, we concluded that cAMP signaling represses *pancNusap1* and *Nusap1* through Icer, leading ultimately to the reduction of *Nusap1* expression via *pancNusap1* downregulation.

Finally, to investigate whether pBiPs other than the *Nusap1* promoter were transcriptionally regulated by downstream transcription factors of the cAMP signaling pathway, we examined the effects of *Icer* and *Creb1* KD on the expression levels of two genes listed next to *Nusap1*: *Arhgap26* and *Gata2* (Figure 4A, Supplementary Table S6). We found that in NcAdiff cells, KD of *Icer* significantly upregulated the expression level of *Arhgap26*, and KD of *Creb1* significantly downregulated the expression level of *Gata2* (Figure S13). These results indicated that *Icer* and *Creb1* were involved in the transcriptional regulation of *Arhgap26* and *Gata2*, respectively, and supported our notion that pBiPs are preferred targets of downstream transcription factors of cAMP signaling during the irreversible differentiation of PC12 cells.

## DISCUSSION

In this study, we utilized PC12 cells as a model for understanding the bidirectional promoter-mediated mechanism underlying cAMP-triggered irreversible differentiation. Genome-wide analysis of our directional RNA-seq dataset and the publicly available pCreb1 ChIP-seq dataset of PC12 cells (15) revealed that bidirectional promoters for the expression of pancRNA–mRNA pairs are preferred downstream targets of cAMP signaling during the irreversible differentiation of PC12 cells. In irreversibly differentiated PC12 cells, the activities of representative bidirectional promoters for the expression of pancRNA–mRNA

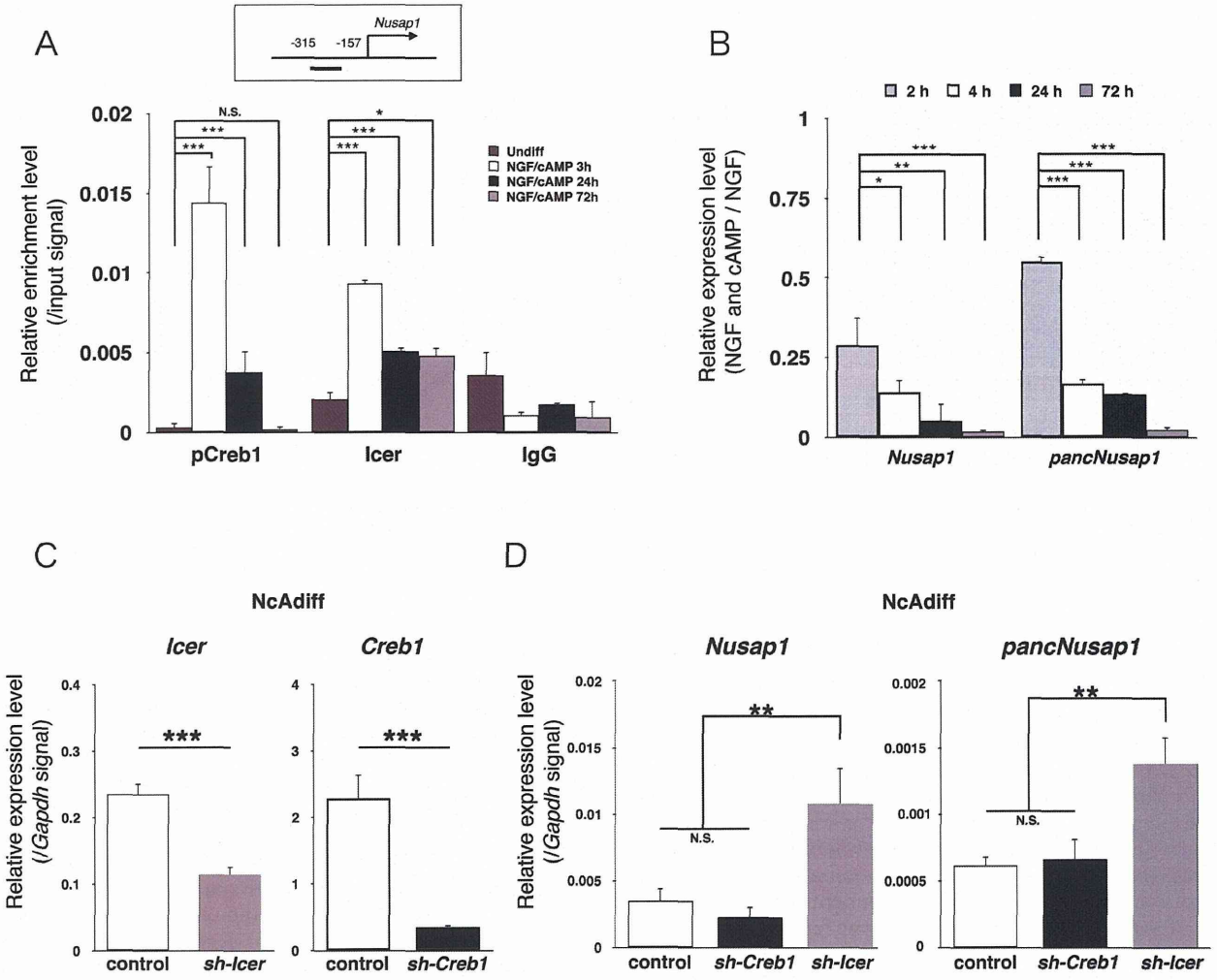


**Figure 8.** The transcriptional activity of *pancNusap1-Nusap1* pair was regulated by Icer after cAMP stimulation. (**A**) pCreb1- and Icer-binding status at the *Nusap1* promoter after 3, 24 and 72 h of NGF/cAMP treatment. Normal rabbit IgG (IgG) was used as a negative control. (**B**) The expression dynamics of *pancNusap1* and *Nusap1* after 2, 4, 24 and 72 h of NGF and/or cAMP treatment. (**C** and **D**) The effects of *sh-Icer* and *sh-Creb* OEs on the expression levels of their target genes (C) and the *pancNusap1-Nusap1* pair (D) in NcAdiff cells. Viral vectors were introduced at day 3. In (A–D), values are mean ± SD ($n = 3$). Statistical analysis was performed using the Tukey-Kramer multiple comparison test. N.S. = not significant. $*P < 0.05$; $**P < 0.01$; $***P < 0.001$.

pairs were regulated by transcription factors in the cAMP-dependent pathway (Figure 8 and Supplementary Figure S13). To examine whether such transcriptional regulation of pancRNA–mRNA pairs contributes to the cAMP-triggered irreversible differentiation, we focused on *pancNusap1* and *Nusap1*, the pancRNA–mRNA pair showing the highest Pearson correlation coefficients of the expression during PC12 differentiation. KD and OE experiments showed that *pancNusap1* positively regulated the *Nusap1* expression in a sequence-specific manner, which was accompanied by acetylation of histone H3 lysine 9 and 27 at the promoter. Both the *pancNusap1* and the *Nusap1* expression levels and the histone acetylation level of the *Nusap1* promoter decreased concomitantly, most likely as part of the regulation responsible for irreversible differentiation, as shown by our finding that the epigenetic silencing of *Nusap1* via KD of *pancNusap1* recapitulated the cAMP effect on cell cycle arrest during the process of irreversible differentiation of PC12 cells.

### Downstream transcription factors of cAMP signaling regulate the expression of hundreds of gene activation-associated ncRNAs derived from bidirectional promoters

A previous ChIP-seq study showed that a quarter of pCreb1-target genes are derived from aBiPs, suggesting that such head-to-head promoter structures may provide adaptive advantages for cAMP functioning in cells (15). In this study, we showed that annotated protein-coding genes were expressed from 474 aBiPs, and from 2718 pBiPs, in rat PC12 cells. Genome-wide analysis, supported by representative experimental tests, revealed that not only aBiPs but